Surface Functionalized Hydrophobic Porous Particles Toward Water Treatment Application

*Alireza Abbaspourrad, Nick J. Carroll, Shin-Hyun Kim, and David A. Weitz**

Porous particles are attractive for applications in drug delivery,[1–3] sensing,[4–6] and absorption of organic pollutants.[7,8] The removal of organic pollutants from undesirable sites, such as the surface of water or a sub-surface aquifer remains a challenge; innovation of materials for effective organic contaminant removal is essential to minimize ecological damage.[9–11] Silica aerogels and core-shell nanoparticles have been used to this end;[12–14] however, due to the hydrophobic nature of their surfaces, these particles are highly unstable in aqueous environments. As a result, the application of these particles has been restricted to air-water interfaces. Effective remediation requires particles which can remain stable in a variety of aqueous environments. A promising route to achieve water dispersion of particles with hydrophobic nature is to tailor the particle surface chemistry: for example, by constructing core-shell particles with a hydrophobic porous oil-absorbing core and a hydrophilic surface to facilitate dispersal in water. Particles that absorb organic contaminants while remaining well dispersed in water are potentially useful for water filtration or purification applications.

In general, these particles must possess three critical features: they should be porous, hydrophobic and coated by a hydrophilic surface. There are various techniques to produce porous particles.[15–17] One flexible and convenient method to form porous particles is the use of pore forming agents known as porogens.[18–20] A highly robust class of porogen processing exploits phase separation of two miscible liquids to produce different domains.[21] By solidifying one of the liquids and selective removal of the second liquid, a porous structure is formed. The porogen-template method is a facile route to produce porous particles; however, the method must be combined with other techniques to produce porous particles with controllable core-shell structure and surface properties. Capillary microfluidic devices have been used to produce core-shell particles using double and single emulsion strategies;[22–28] for example, by controlling the spreading of two immiscible oils in a continuous phase to form core-shell structures.[29] However, these methods have not yet been investigated for fabrication of porous core-shell particles designed with controllable surface properties. Thus, the fabrication of hydrophobic porous particles tailored for aqueous dispersion remains an important yet unmet need.

In this paper, we introduce a new type of porous core-shell particle designed to uptake organic contaminants in aqueous solution. We use microfluidic and porogen templating techniques to fabricate particles with a hydrophobic porous core and a hydrophilic surface. The hydrophilic surface enables the particles to be dispersed in water, while the hydrophobic core absorbs organic molecules from the surrounding aqueous environment. We use a capillary microfluidic device to prepare paired droplets consisting of two photocurable monomer mixtures dispersed in an aqueous continuous phase. To lower interfacial energy, the less hydrophobic monomer mixture spontaneously spreads and engulfs the more hydrophobic mixture to form a non-centric core-shell droplet. The monomer mixture which spreads to form the shell contains hydrophilic silica nanoparticles; the nanoparticles adsorb at the aqueous interface and confer hydrophilicity to the particle surface for dispersion in water. The inner mixture is a binary blend of photocurable monomer and porogen PDMS template. We form porous particles by photopolymerizing the monomers and subsequently removing the template porogen. These surface-modified particles demonstrate a good ability to absorb organic contaminants from an aqueous environment while remaining well dispersed in the water phase.

To synthesize particles, we emulsify two different monomer mixtures into single drops in an aqueous continuous phase using a glass capillary microfluidic device. The device is constructed from a theta (θ) shaped injection capillary which has two separate channels. We taper the theta (θ) shaped capillary and insert it inside a cylindrical collection capillary to increase the velocity of the continuous phase by confining the flow near the tip of the injection capillary. Both theta (θ) shaped and cylindrical capillaries are placed coaxially inside a square capillary whose inner dimension is the same as that of the outer diameter of the theta shaped and cylindrical capillaries; a schematic of the device is shown in **Figure 1**a. We flow monomer of ethoxylated trimethylolpropane triacrylate (ETPTA) containing 1 wt.% silica nanoparticles through one channel of the θ-shaped capillary and isobornylmethaacrylate (IBMA) plus PDMS oil and a crosslinker (hexandiol dimethylacrylate) through the second channel, as shown in Figure 1b. We refer to the IBMA, PDMS and crosslinker as IBMA mixture. We introduce the continuous phase by pumping an aqueous surfactant solution of

Dr. A. Abbaspourrad, Dr. N. J. Carroll,
Prof. D. A. Weitz
Harvard University
School of Engineering and Applied Sciences
and Department of Physics
29 Oxford Street, Cambridge, MA 02138, USA
E-mail:weit z@seas.harvard.edu
Dr. S.-H. Kim
Harvard University
School of Engineering and Applied Sciences and Department of Physics
29 Oxford Street, Cambridge
MA 02138, USA
Department of Chemical and Biomolecular Engineering
KAIST, Daejeon, South Korea

DOI:10. 1002/adma.201300656

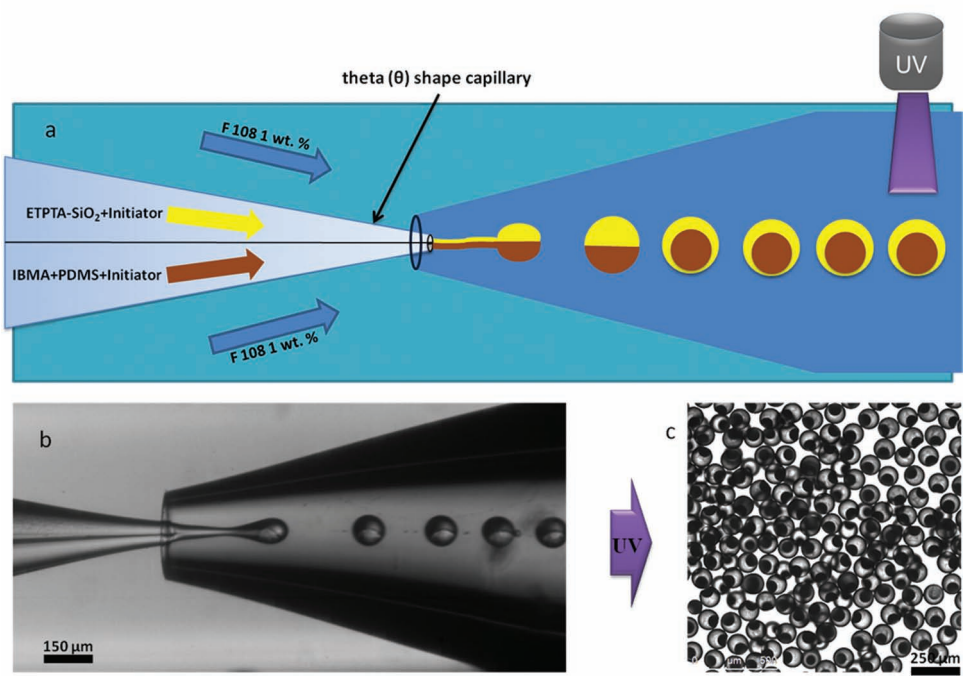

Figure 1. a) Schematic illustration of the microfluidic device comprised of a tapered theta (θ)-shaped capillary for injection of two oil phases and a circular capillary for droplet collection. b) Optical microscope image showing droplet generation in dripping mode. c) Optical microscope image of resultant multilayer particles following UV exposure.

1 wt% ethylene oxide-propylene oxide-ethylene oxide triblock copolymer (Pluronic F-108) through the interstices of the square and cylindrical capillaries. We generate drops consisting of two different monomer mixtures; the upper phase is ETPTA with dispersed silica particles while the lower phase is the IBMA mixture, as shown in Figure 1a. The ETPTA phase completely wets the surface of the IBMA mixture, forming a non-centric core-shell drop as shown in Figure 1a and Movie S1. The complete coverage occurs because the spreading of ETPTA reduces the interfacial area of high surface tension between the IBMA mixture and water. The ETPTA phase contains hydrophilic silica particles which spontaneously adsorb to the interface with water, where they minimize the total interfacial energy by reducing the contact area between ETPTA and water. The particles remain trapped at the ETPTA/water interface because the reduction of interfacial energy is much greater than thermal energy.

Following droplet generation, ETPTA spreads on the surface and mixes with the IBMA and PDMS in the core. Due to the low miscibility of ETPTA and PDMS, a mixture-driven phase separation occurs within the droplet; thus, PDMS phase separates from the mixture resulting in formation of a PDMS-rich inner layer surrounded by a monomer-rich middle layer. Both layers consist of a binary blend of photocurable monomers and porogen PDMS. However, the PDMS-rich inner layer is distinguished by a much larger ratio of porogen PDMS to monomer in comparison with the middle layer. The outermost layer of the drop is comprised of silica nanoparticles dispersed within monomer mixture. A diagram illustrating the droplet layers is shown in the first step of **Figure 2**a. We prepare porous particles by in situ photopolymerization of the multi-layered droplets containing porogen PDMS. The difference in porogen to monomer ratio within the monomer-rich and PDMS-rich layers results in the formation of dissimilar polymeric structures within each layer. In the PDMS-rich layer, the precipitation polymerization of monomers results in inter-connected polymeric particles whose sub-micron interstices are filled with PDMS. By contrast, polymerization of the monomer-rich middle layer leads to the exclusion of PDMS to nanometer size domains dispersed within a continuous polymeric matrix. Polymerized regions are shown as amber color while dark brown color represents porogen PDMS in the second step of Figure 2a. To replace liquid PDMS with air we wash the particles with isopropanol (IPA) and subsequently dry them. Air-filled pores are represented with white color as shown in the last step of Figure 2a.

We cut the prepared multilayered particles in half and obtain SEM images to examine the surface and internal structure. At the surface, anchored silica particles form hexagonal arrays over the entire exterior of the microparticle, as shown in the SEM image in Figure 2b. A high magnification SEM image of the protruding silica particles, 380 nm in diameter, is shown in the inset of Figure 2b. The outer layer is characterized by a polymer matrix enriched with dispersed hydrophilic silica particles as shown in Figure 2c. Functionalization with colloidal silica confers surface hydrophilicity to the particles which facilitates dispersal in water. By contrast, the porous structure of the hydrophobic middle and inner layers is designed to absorb organic molecules. The middle layer is characterized by small pores of tens of nanometers in size, as shown in Figure 2d; a high magnification SEM image of the middle layer polymeric nanostructure is also shown in Figure S1 in the Supporting Information. The inner layer is comprised of interconnected IBMA spheres characterized by larger pores with dimensions of hundreds of nanometers, as shown in Figure 2e.

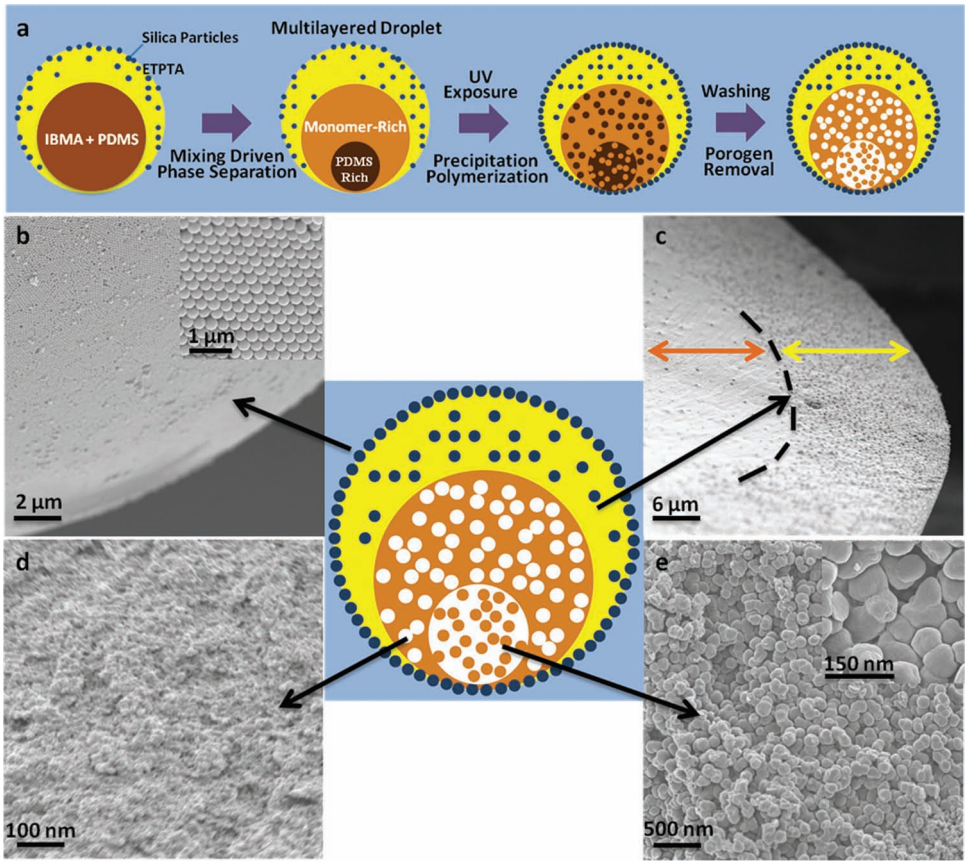

Figure 2. a) Schematic illustration describing the mechanism of mixing driven phase separation, precipitation polymerization and subsequent pore formation after removal of porogen PDMS oil. b-e) SEM images of the surface and the three different layers within the porous particle.

The multilayered droplets which act as templates for our porous particles likely form by phase separation of the ETPTA, IBMA, and PDMS mixture. To test this hypothesis, we use bulk mixtures of these three fluids to determine their ternary phase diagram; the phase boundary is shown by the dashed line within the phase diagram in **Figure 3**. For small concentrations of ETPTA and PDMS, the fluids mix homogeneously, as indicated by the blue points in Figure 3. By contrast, for sufficiently large ETPTA and PDMS concentrations, the fluids do not mix homogeneously; instead, they phase-separate into PDMS-rich and monomer-rich phases, as indicated by the red points in Figure 3. Clearly, to form multilayered droplets which act as templates for our porous particles, the droplet fluid composition must fall within the two phase region; this is achieved by adjusting the relative flow rates of ETPTA and IBMA/PDMS mixture. In this case, phase separation within the droplet initiates upon component mixing to form PDMS-rich and monomer-rich layers; eventually, phase separation will proceed to completion

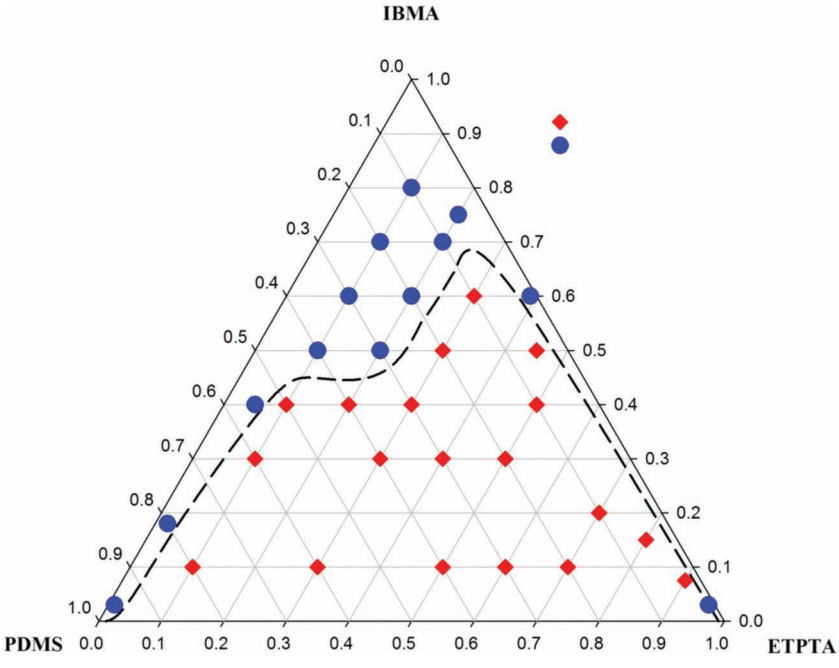

Figure 3. ETPTA, IBMA and PDMS Ternary phase diagram, the phase boundary is indicated by the dashed line.

resulting in a multi-layered equilibrium structure. The molar ratio of porogen to monomer is constant as predetermined by the flow rates of fluids injected to form the droplet; however, as phase separation proceeds within the droplet, this ratio increases within the droplet inner layer while concurrently decreasing within the droplet middle layer. Therefore, the time interval between droplet generation and UV exposure is critical; it determines the final porogen to monomer ratio at the time of polymerization and thus the corresponding polymeric nanostructures formed. In our case, we arrest phase separation a few seconds after droplet generation by in situ photopolymerization to obtain the desired microstructures; thus, adjusting the interval between droplet generation and UV exposure, could in principle, provide an additional level of design control for these porous particles.

To approximate the porogen to monomer ratio within the highly porous inner layer at the time of *in-situ* photopolymerization, we prepare various combinations of IBMA monomer and porogen in bulk. We photopolymerize the mixtures, subsequently remove the porogen PDMS, and examine the resultant porous structures within the bulk polymeric matrix using SEM. The pores within the polymer matrix become larger in size as the porogen to monomer ratio increases, as shown by the SEM images in Figure S2. By comparing the structures formed in bulk with that of the microparticles, we estimate the ratio of porogen to monomer within the inner layer at the time of in-situ polymerization as 1:1. Using our approach, the porogen to monomer ratio and corresponding particle internal microstructure can be controlled by adjusting mixture composition and time interval between droplet generation and UV exposure.

Despite its applicability to tailoring porous structures by controlling the extent of phase separation, our technique is limited to relatively short time intervals between drop generation and UV irradiation. We observe in the case of long time intervals, phase separation proceeds to completion and, due to the low monomer content within the PDMS-rich inner layer, no consolidated structure can be formed within the inner layer upon UV exposure. To substantiate this observation, we generate drops and store them for 12 hours and subsequently photopolymerize them. Following washing steps, we image the particles using SEM. We observe a 45 μm diameter cavity at the particle surface as evidenced by Figure S3a; a higher magnification SEM image is shown in Figure S3b. This result illustrates the importance of the time interval between droplet generation and photopolymerization for fabricating particles with controlled microstructure using this technique. We also control the size of the porous inner layer by varying the relative volumetric flow rates of the ETPTA (Q_1) and IBMA/PDMS (Q_2) mixtures. Operating in the dripping mode, we adjust the size of the inner layer with three different relative flow rates of $Q_1/Q_2 = 0.6$, $Q_1/Q_2 = 1$ and $Q_1/Q_2 = 1.5$, while maintaining a constant sum of Q_1 and Q_2. Optical microscope images of the resultant microparticles are shown in the left and middle columns of **Figures 4**a–c with SEM images in the right column. In the optical images,

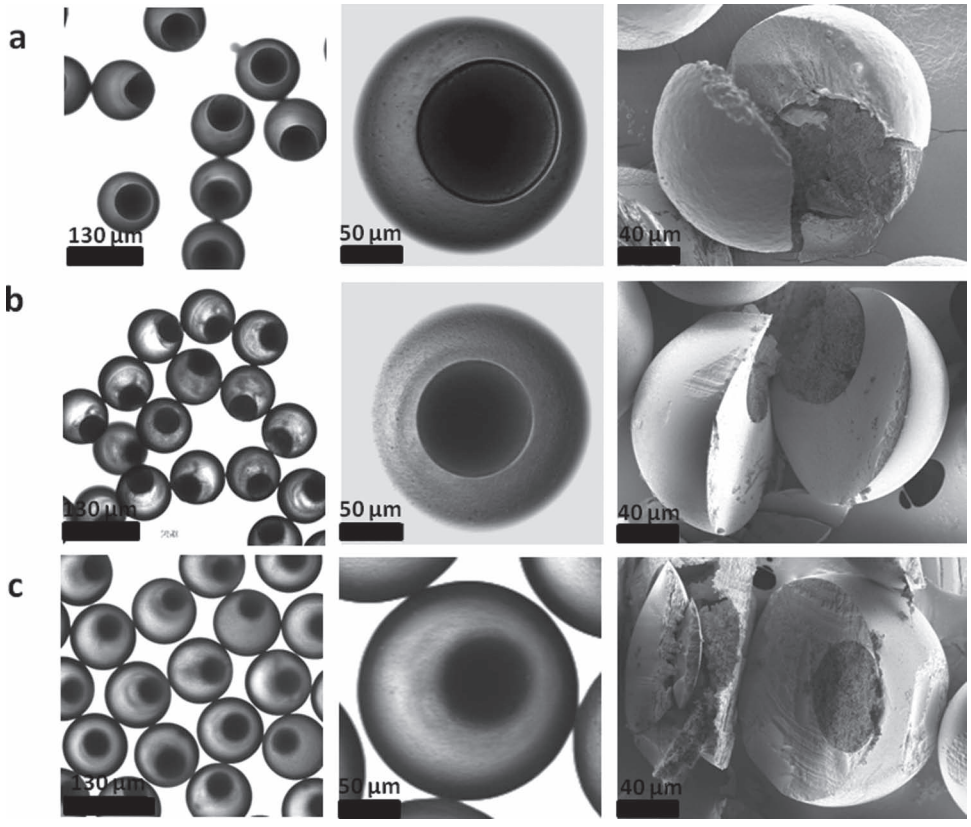

Figure 4. Optical microscope (left and middle column) and SEM images (right column) of particles formed using three different relative volumetric flow rate ratios of ETPTA (Q_1) and IBMA mixture (Q_2). a) $Q_1/Q_2 = 0.6$; b) $Q_1/Q_2 = 1$; c) $Q_1/Q_2 = 1.5$.

we observe a distinct dark sphere inside the particle, which is the porous inner layer; this high opacity is caused by strong light scattering in the heterogeneous inner layer structure. Using SEM, we are also able to confirm that the size of the inner core region increases with increasing ratios of Q_1/Q_2. Adjusting the relative flow rate offers a simple and effective way to tailor the size of the hydrophobic porous inner layer.

To demonstrate the effectiveness of our porous particles to absorb organic contaminants, we immerse them in an aqueous solution saturated with decane hydrocarbon oil and subsequently measure the amount of oil absorbed. We place dried porous particles (Q_1/Q_2 = 0.6) within a glass vial and set a paper filter on top of the particles to prevent them from rising. To prepare an aqueous solution saturated with organic contaminants, we add a water layer to the bottom of the vial followed by gentle addition of a decane oil layer on top of the water surface. After sealing the vial, we incubate the samples at 65 ° C for predetermined amounts of time. We then dry the particles and subsequently weigh them to measure the amount of hydrocarbon oil absorbed at different intervals over a 52 h time period as shown in **Figure 5**a. The maximum amount of absorbed oil reaches 16 wt.% of the initial particle sample weight at 48 hours; no significant increase in oil uptake is measured after 48 hours as evidenced by the black squares in Figure 5a. Remarkably, despite the intrinsic hydrophobic nature of the porous particles, they remain stable and well dispersed in water throughout the experiment; we attribute the excellent dispersion of the particles to the designed hydrophilic surface. This result illustrates the potential of surface-functionalized porous particles as effective organic contaminant absorbers in aqueous environments. The significance of nanopores for effective contaminant absorption is substantiated by an implementation of the preceding experiment using non-porous particles of the same material; these particles are constructed using our fabrication method, the only difference being exclusion of PDMS porogen. In this case, the particles absorb only 1.7 wt% of their initial weight over 52 hours as evidenced by the red circles in Figure 5a; this considerable reduction in the absorption capacity illustrates the importance of the porous nanostructures obtained by porogen templating. In the case of water-dispersed porous particles, the air-filled pores result in an opaqueness of the inner layer as characterized by optical microscopy in transmission mode. Mie scattering dominates because of the high contrast in refractive indices between air (n_{air} = 1) and IBMA particles (n_{IBMA} = 1.47) within the inner layer. As decane oil molecules (n_{decane} = 1.49) are absorbed, the contrast decreases, resulting in diminished scattering and increased transparency. We image the particles using an optical microscope and observe a change in the brightness of the inner layer as time proceeds. At 48 h core becomes transparent, after which no significant changes are observed. Microscope images of a particle core increasing in brightness at different time intervals are shown in Figure 5c.

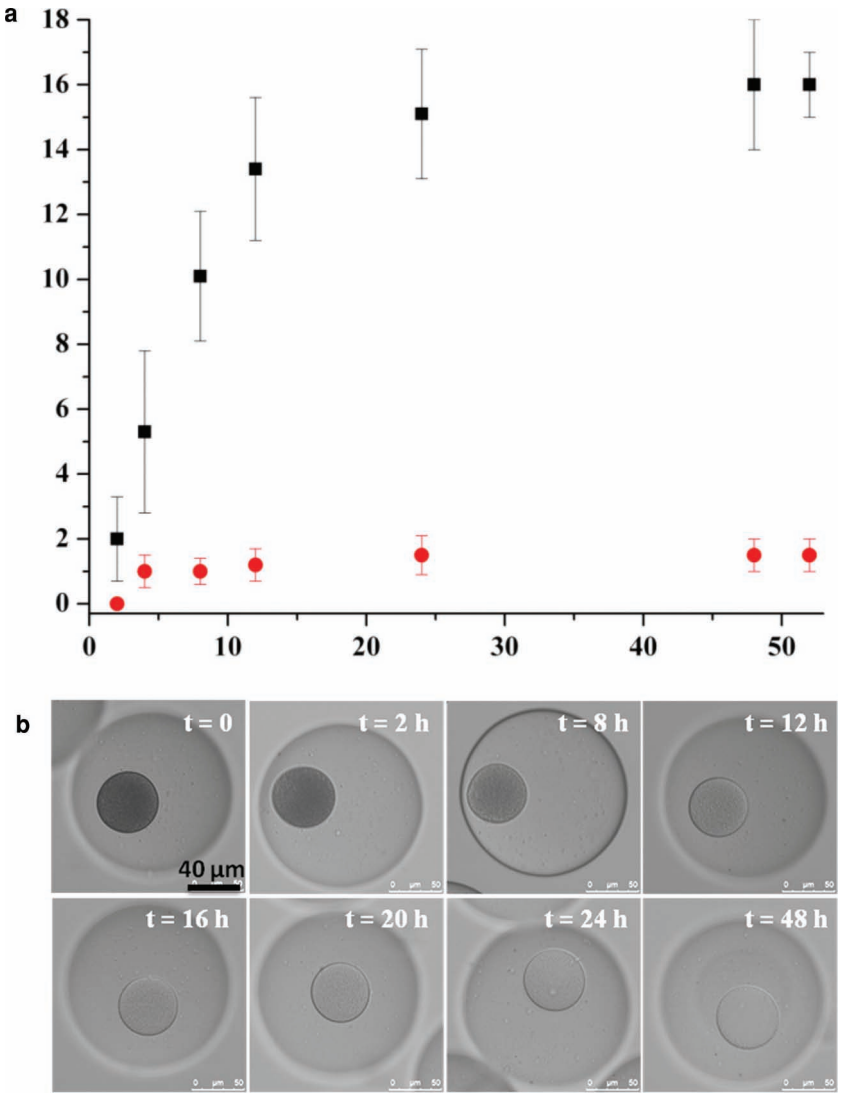

Figure 5. a) The amount of oil absorbed as characterized by measuring particle weight over time for porous particles (black squares) and non-porous particles (red circles). b) Optical images series of particles absorbing oil and consequent increase of inner layer brightness during 48 h time period.

In addition to absorption, the desorption capacity of the particles is an important feature for practical use in water treatment applications. To demonstrate the recycling capability of our particles, we remove the absorbed organic oil by immersing the particles in IPA solution at 60 °C for ten minutes. Thereafter, the particles are dried and reweighed; the weight of the recycled particles is the same as the weight measured prior to their use in the preceding water treatment experiment. Moreover, we observe an opaque inner layer within the dried particles which

further suggests effective removal of the organic contaminant from the pores. We then repeat the water treatment experiment using the recycled particles to measure their absorbance capacity. The amount of organic contaminants absorbed by the recycled particles after 52 h of exposure is 16 wt.% of the initial particle sample weight. This result demonstrates simple recycling of the particles with reasonable time scale for both the contaminant absorption and desorption processes. To enhance their applicability for water treatment applications, it is desirable to retrieve the particles after organic contaminant uptake. To facilitate their recovery, we functionalize the particles using iron oxide magnetic nanoparticles. We disperse 0.1 wt% of iron oxide nanoparticles stabilized by oleic acid (Sigma-Aldrich) in ETPTA monomer to fabricate magnetic-responsive particles. Upon applying an external magnetic force, the particles respond and translate in the direction of the applied field as shown in Movie S2.

The versatility of our porous particles is further demonstrated by dispersing them in an oil-in-water emulsion to absorb organic molecules directly from the surface of oil drops. We disperse particles in water; these particles are characterized by an opaque core as shown in **Figure 6**a. After addition of hydrocarbon oil, we shake the vial to form oil drops suspended in water. The particles assemble at oil-water interfaces and begin to uptake oil as shown in the optical image in Figure 6b. However, they remain at the interface and do not partition into the oil drops; we attribute this behavior to the designed hydrophilic surface of the particles. We use optical microscopy to verify the complete coverage of an oil droplet at different focal planes as shown in Movie S3. Interestingly, we observe that within minutes, small spherical oil droplets become non-spherical as highlighted by dashed-lines in Figure 6c. The non-spherical oil droplets form because of volume depletion due to oil uptake and subsequent particle jamming at the interface. Two different circular lines are observed at the particle surface as shown in Figures 6d,e. The smaller circle is the inner layer of the particle whose brightness increases as oil is absorbed, and the larger circle is the contact line of the particle protruding into the oil droplet. We observe that as the particles absorb oil, the inner layers transform from an initially opaque to a bright appearance within minutes as shown in Figure 6f. We observe the time for oil uptake is faster from an oil drop surface than an aqueous solution containing dissolved oil. We thus demonstrate that the particles are not limited to organic molecule uptake from aqueous solution, they can also anchor to oil surfaces and quickly absorb hydrocarbons in the case of direct contact with oil droplets. Our work shows that by selective tuning of particle core and surface properties, fabrication of organic contaminant absorbing particles which remain well dispersed in water can be achieved.

In this paper, we present a pragmatic approach to fabricate core-shell particles which absorb organic molecules while remaining well-dispersed in aqueous solution. We combine microfluidics, mixing-induced phase separation, and precipitation polymerization to engineer particles with a hydrophobic porous core and hydrophilic shell. The hydrophobic porous core is designed to uptake organic contaminants while the hydrophilic shell confers excellent dispersion of particles in an aqueous phase. We tune the surface properties of the core-shell particles by including silica nanoparticles at the particle surface with different degrees of hydrophilicity. Furthermore, we demonstrate the effectiveness of the particles to absorb organic

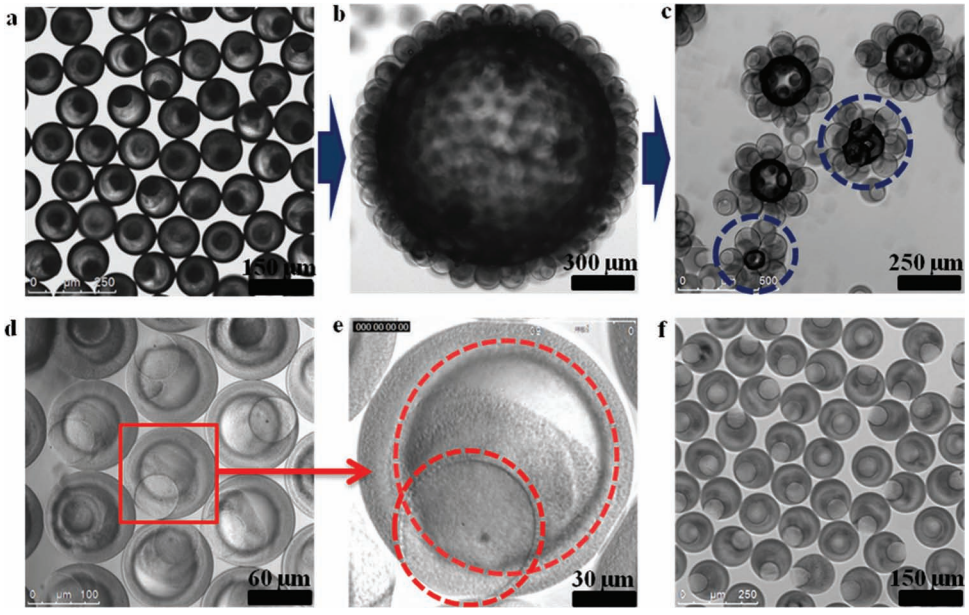

Figure 6. a) Optical microscope images of porous particles with opaque cores before oil uptake. b) Particles anchored at the surface of an oil droplet. c) Oil droplets become non-spherical due to volume depletion and particle jamming as a result of oil absorption by the porous particles. d,e) Optical microscope images of oil absorbing particles showing the contact line (large circle) and inner layer (small circle). f) Optical microscope image of particles with bright cores after oil uptake and recovery.

oil directly from oil drops. Moreover, the ability of these particles to uptake organic molecules is not limited to direct contact with oil; they can also absorb organic molecules dissolved in an aqueous solution. We characterize the amount of organic contaminant absorbed by weight. By adjusting the size of the core and its porosity we can enhance the amount of organic molecules absorbed. We demonstrate a simple approach for the recycling and reuse of these absorbing porous particles. Moreover, we functionalize core-shell particles using iron oxide nanoparticles to facilitate their retrieval after contaminant absorption. Our work represents an important step towards fabrication of functionalized particles which can absorb organic contaminants while remaining well dispersed in aqueous solution. These particles demonstrate great promise for practical use in water treatment applications.

Supporting Information

Supporting Information is available from the Wiley Online Library or from the author.

Acknowledgements

This work was supported by the Advanced Energy Consortium. Member companies include BP America Inc., Baker Hughes Inc., Conoco-Phillips, Halliburton Energy Services Inc., Marathon Oil Corp., Occidental Oil and Gas, Petrobras, Schlumberger, Shell, and Total.

Received: February 7, 2013
Published online: May 6, 2013

[1] M. Vallet-Regí, F. Balas, D. Arcos, *Angew. Chem., Int. Ed.* **2007**, *46*, 7548–7558.
[2] I. I. Slowing, B. G. Trewyn, V. S.-Y. Lin, *J. Am. Chem. Soc.* **2007**, *129*, 8845–8849.
[3] Y. Yang, N. Bajaj, P. Xu, K. Ohn, M. D. Tsifansky, Y. Yeo, *Biomaterials* **2009**, *30*, 1947–1953.
[4] S. Chan, P. M. Fauchet, Y. Li, L. J. Rothberg, B. L. Miller, *Phys. Status Solidi A – Appl. Res.* **2000**, *182*, 541–546.
[5] J. Zhang, X. Liu, S. Wu, M. Xu, X. Guo, S. Wang, *J. Mater. Chem.* **2010**, *20*, 6453–6459.
[6] C. Sun, S. Rajasekhara, Y. Chen, J. B. Goodenough, *Chem. Commun.* **2011**, *47*, 12852–12854.
[7] N. Kawabata, Y. Tsuchida, Y. Nakamori, M. Kitamura, *Reactive Funct. Polym.* **2006**, *66*, 1641–1648.
[8] P. B. Hatzinger, M. Alexander, *Environ. Toxicol. Chem.* **1997**, *16*, 2215–2221.
[9] M. O. Adebajo, R. L. Frost, J. T. Kloprogge, O. Carmody, S. Kokot, *J. Porous Mater.* **2003**, *10*, 159–170.
[10] O. Carmody, R. Frost, Y. Xi, S. Kokot, *J. Thermal Anal. Calorimetry* **2008**, *91*, 809–816.
[11] C. Yang, U. Kaipa, Q. Z. Mather, X. Wang, V. Nesterov, A. F. Venero, M. A. Omary, *J. Am. Chem. Soc.* **2011**, *133*, 18094–18097.
[12] J. G. Reynolds, P. R. Coronado, L. W. Hrubesh, *J. Non-Crystalline Solids* **2001**, *292*, 127–137.
[13] V. G. Parale, D. B. Mahadik, M. S. Kavale, A. V. Rao, P. B. Wagh, S. C. Gupta, *Soft Nanosci. Lett.* **2011**, *1*, 97–104.
[14] Q. Zhu, F. Tao, Q. Pan, *App. Mat. Interfaces* **2010**, *2*, 3141–3146.
[15] H. Zhang, X.-J. Ju, R. Xie, C.-J. Cheng, P.-W. Ren, L.-Y. Chu, *J. Colloid Interface Sci.* **2009**, *336*, 235–243.
[16] T. K. Kim, J. J. Yoon, D. S. Lee, T. G. Park, *Biomaterials* **2006**, *27*, 152–159.
[17] Y. Baimark, *Polymer* **2009**, *50*, 4761–4767.
[18] F.-C. Huang, C.-H. Ke, C.-Y. Kao, W.-C. Lee, *J. Appl. Polym. Sci.* **2001**, *80*, 39–46.
[19] R. Wang, Y. Zhang, G. Ma, Z. Su, *Colloids Surf. B: Biointerfaces* **2006**, *51*, 93–99.
[20] D. Horak, J. Labsky, J. Pilar, M. Bleha, Z. Pelzbauer, F. Svec, *Polymer* **1993**, *34*, 3481–3489.
[21] H. Matsuyama, T. Iwatani, Y. Kitamura, M. Tearamoto, N. Sugoh, *J. Appl. Polym. Sci.* **2001**, *79*, 2449–2455.
[22] F. Tu, D. Lee, *Langmuir* **2012**, *28*, 9944–9952.
[23] D. Lee, D. A. Weitz, *Adv. Mater.* **2008**, *20*, 3498–3503.
[24] R. K. Shah, H. C. Shum, A. C. Rowat, D. Lee, J. J. Agresti, A. S. Utada, L.-Y. Chu, J.-W. Kim, A. Fernandez-Nieves, C. J. Martinez, D. A. Weitz, *Mater. Today* **2008**, *11*, 18–27.
[25] A. S. Utada, L.-Y. Chu, A. Fernandez-Nieves, D. R. Link, C. Holtze, D. A. Weitz, *MRS Bull.* **2007**, *32*, 702–708.
[26] S.-H. Kim, J.-W. Kim, J.-C. Cho, D. A. Weitz, *Lab Chip* **2011**, *11*, 3162–3166.
[27] R. K. Shah, J.-W. Kim, J. J. Agresti, D. A. Weitz, L.-Y. Chu, *Soft Matter* **2008**, *4*, 2303–2309.
[28] L. Liu, J.-P. Yang, X.-J. Ju, R. Xie, Y.-M. Liu, W. Wang, J.-J. Zhang, C. H. Niu, L.-Y. Chu, *Soft Matter* **2011**, *7*, 4821–4827.
[29] S.-H. Kim, A. Abbaspourrad, D. A. Weitz, *J. Am. Chem. Soc.* **2011**, *133*, 5516–5525.